



HAL
open science

On the survival of zombie vortices in protoplanetary discs

Geoffroy R. J. Lesur, Henrik Latter

► **To cite this version:**

Geoffroy R. J. Lesur, Henrik Latter. On the survival of zombie vortices in protoplanetary discs. Monthly Notices of the Royal Astronomical Society, 2016, 462, pp.4549-4554. 10.1093/mnras/stw2172 . insu-03691482

HAL Id: insu-03691482

<https://insu.hal.science/insu-03691482>

Submitted on 9 Jun 2022

HAL is a multi-disciplinary open access archive for the deposit and dissemination of scientific research documents, whether they are published or not. The documents may come from teaching and research institutions in France or abroad, or from public or private research centers.

L'archive ouverte pluridisciplinaire **HAL**, est destinée au dépôt et à la diffusion de documents scientifiques de niveau recherche, publiés ou non, émanant des établissements d'enseignement et de recherche français ou étrangers, des laboratoires publics ou privés.

On the survival of zombie vortices in protoplanetary discs

Geoffroy R. J. Lesur^{1,2★} and Henrik Latter³

¹CNRS, IPAG, F-38000 Grenoble, France

²Univ. Grenoble Alpes, IPAG, F-38000 Grenoble, France

³DAMTP, University of Cambridge, CMS, Wilberforce Road, Cambridge CB3 0WA, UK

Accepted 2016 August 2. Received 2016 July 31; in original form 2016 June 3

ABSTRACT

Recently it has been proposed that the zombie vortex instability (ZVI) could precipitate hydrodynamical activity and angular momentum transport in unmagnetized regions of protoplanetary discs, also known as ‘dead zones’. In this Letter we scrutinize, with high-resolution 3D spectral simulations, the onset and survival of this instability in the presence of viscous and thermal physics. First, we find that the ZVI is strongly dependent on the nature of the viscous operator. Although the ZVI is easily obtained with hyperdiffusion, it is difficult to sustain with physical (second order) diffusion operators up to Reynolds numbers as high as 10^7 . This sensitivity is probably due to the ZVI’s reliance on critical layers, whose characteristic length-scale, structure, and dynamics are controlled by viscous diffusion. Second, we observe that the ZVI is sensitive to radiative processes, and indeed only operates when the Peclet number is greater than a critical value $\sim 10^4$, or when the cooling time is longer than $\sim 10\Omega^{-1}$. As a consequence, the ZVI struggles to appear at $R \gtrsim 0.3$ au in standard $0.01 M_{\odot}$ T Tauri disc models, though younger more massive discs provide a more hospitable environment. Together these results question the prevalence of the ZVI in protoplanetary discs.

Key words: hydrodynamics – instabilities – protoplanetary discs.

1 INTRODUCTION

The origin of angular momentum transport in accretion discs, especially protoplanetary discs, is a long-standing issue in the astrophysical community. Angular momentum transport is the mechanism that governs the global dynamics of the gas, in particular its accretion on to the central star. It is therefore especially important if one is to predict the long-term evolution and structure of protoplanetary discs.

The magnetorotational instability (MRI; Balbus & Hawley 1991) is believed to be the main driver of angular momentum transport in accretion discs. By sustaining three-dimensional magnetohydrodynamics (MHD) turbulence, the MRI transports angular momentum outwards and leads to mass accretion at rates compatible with observations. It is far from assured, however, that cold protoplanetary discs are sufficiently ionized to sustain MHD turbulence. This has led to the concept of ‘dead zones’ (Gammie 1996), internal regions of the disc where the MRI is quenched. The question of angular momentum transport in dead zones is highly debated, and in which hydrodynamical instabilities are likely to be key (Turner et al. 2014).

The radial Keplerian rotation profile of astrophysical discs is known to be hydrodynamically stable, both linearly and non-linearly (Lesur & Longaretti 2005; Edlund & Ji 2014). However, additional

physics, such as cooling, heating, and stratification, could unleash new hydrodynamical instabilities. In recent years, several have been identified, including the subcritical baroclinic instability (SBI; Petersen, Julien & Stewart 2007; Lesur & Papaloizou 2010), the vertical shear instability (VSI; Nelson, Gressel & Umurhan 2013), the convective overstability (Klahr & Hubbard 2014), and more recently the zombie vortex instability (ZVI) which appears in rotating shear flows exhibiting a stable vertical stratification.

The ZVI was first observed (but not clearly identified as such) in the anelastic simulations of Barranco & Marcus (2005) and was subsequently isolated by Marcus et al. (2013) using Boussinesq spectral simulations. This instability, of non-linear nature, produces ‘self-replicating’ vortices thanks to the excitation of very thin critical layers. The ZVI also appears in compressible simulations with various initial conditions. It has been proposed, but not yet demonstrated, that the excitation of spiral density waves by zombie vortices could lead to significant angular momentum transport in dead zones (Marcus et al. 2015), thereby solving the angular momentum transport problem in these regions. However, the physical mechanism driving the instability remains mysterious. The existence and excitation of critical layers by a perturbation is a well-known linear mechanism in shear flows (Drazin & Reid 1981), but their non-linear saturation and spontaneous transformation into new vortices is largely unexplained. Recently, based on a linear and a quasi-linear analysis, Umurhan, Shariff & Cuzzi (2016) proposed that critical layers could be subject to a stratified variant of the Rossby wave

* E-mail: geoffroy.lesur@univ-grenoble-alpes.fr

instability (Lovelace et al. 1999). However, this scenario needs to be supplemented with a mechanism to self-sustain the original perturbation, and further tested with more realistic non-linear models of the layer, including viscous effects. Indeed, because diffusive physics determines the layer's structure and evolution, the nature of viscosity (and whether it is physical or numerical) should be a fundamental ingredient in any theory.

In this Letter, we scrutinize the foundations of the ZVI with our focus squarely on the role of viscosity and cooling. We first present our physical model and numerical methods, which are very similar to Marcus et al. (2013). We then move to the question of the physical convergence of the ZVI as a function of the viscous operator. We also explore the dependence of the ZVI on cooling, and compare our results to realistic protoplanetary disc models. We finally summarize our results and propose future routes of research into the ZVI.

2 METHODS

2.1 Physical model

We represent the local dynamics of the disc with the shearing box approximation. To further simplify the dynamics, we employ incompressibility but include vertical buoyancy effects via the Boussinesq approximation. In this framework, the equations of motion read

$$\frac{\partial \mathbf{u}}{\partial t} + \mathbf{u} \cdot \nabla \mathbf{u} = -\nabla \Pi - 2\boldsymbol{\Omega} \times \mathbf{u} + 2\Omega S x \mathbf{e}_x - N^2 \theta \mathbf{e}_z + \nu \Delta \mathbf{u} + (\nu_6 \nabla^2)^3 \mathbf{u}, \quad (1)$$

$$\frac{\partial \theta}{\partial t} + \mathbf{u} \cdot \nabla \theta = u_z + \chi \Delta \theta + (\chi_6 \nabla^2)^3 \theta - \frac{\theta}{t_c}, \quad (2)$$

$$\nabla \cdot \mathbf{u} = 0. \quad (3)$$

In the above formulation we have defined the local rotation frequency Ω , the shear rate S , the Brunt–Vaissala frequency N , and the generalized pressure Π , which allows us to satisfy the incompressible condition (3). In addition, we have introduced several explicit diffusion operators: the usual second-order viscosity ν and thermal diffusivity χ are supplemented with sixth-order ‘hyperdiffusion’ operators with coefficients ν_6 and χ_6 . Hyperdiffusion has no real physical motivation but can be useful numerically to reduce diffusion on large scales without accumulating energy at the grid scale. Note that a similar hyperdiffusion operator was used by Marcus et al. (2015). Finally, we have added a Newtonian cooling in the form of a constant thermal relaxation time t_c .

The above set of equations admits a simple solution of pure shear flow $\mathbf{u}_0 = -Sx\mathbf{e}_y$. In the following, we define perturbations (not necessarily small) to this global shear flow $\mathbf{v} = \mathbf{u} - \mathbf{u}_0$.

The equations of motions are supplemented by a set of periodic boundary conditions in the y and z directions. In the x direction, we use shear-periodic boundary conditions, following Hawley, Gammie & Balbus (1995).

2.2 Dimensionless numbers and units

The set of equations above includes several dynamical time-scales that can be usefully compared via appropriate dimensionless numbers. We define and use the following ones.

(i) The Rossby number $q = S/\Omega$. In Keplerian accretion discs $q = 3/2$, which will be the framework of this Letter.

(ii) The Froude number $\text{Fr} = N/\Omega$. In this work, we will always assume $\text{Fr} = 2$ which corresponds to the fiducial case studied by Marcus et al. (2013) of a moderately stratified flow. Note however that expected Froude numbers in protoplanetary discs are somewhat lower than this value, with $\text{Fr} \simeq 0.3$ (Dubrulle et al. 2005). Our set-up therefore represents an upper bound on the amplitude of stratification effects.

(iii) The Reynolds number $\text{Re} = \Omega L^2/\nu$ compares the amplitude of non-linear advection terms to viscous diffusion. Equivalently, we define a Reynolds number based on hyperviscosity $\text{Re}_6 = \Omega^{1/3} L^2/\nu_6$.

(iv) The Peclet number $\text{Pe} = \Omega L^2/\chi$ compares non-linear advection to thermal diffusion. As for the Reynolds number, we also define a hyperdiffusion Peclet number Pe_6 .

(v) The dimensionless cooling time $\tau = t_c \Omega$.

Unless mentioned otherwise, we use Ω^{-1} as our time unit and the box size L as our length unit.

2.3 Numerical technique

We employ `SNOOPY` to integrate the equations of motion. `SNOOPY` is a spectral code using a Fourier decomposition of the flow to compute spatial derivatives. Time integration is performed using a low storage third-order Runge–Kutta scheme. Diffusive operators are solved by an implicit operator which maintains the third-order accuracy of the scheme. To avoid spectral aliasing due to the quadratic nonlinearities, we use a standard 2/3 anti-aliasing rule when computing each non-linear term. The code and ZVI set-up is freely available on the author's web site.

In this Letter, we use two sets of initial condition: single vortex initial conditions (runs label ending with ‘v’) and Kolmogorov-like noise (runs label ending with ‘k’).

Our single vortex initial condition is similar to Marcus et al. (2013) with an isolated Gaussian vortex centred at the origin of the box with a size σ and a velocity amplitude v_0 . The initial perturbation reads

$$v_x^0(\mathbf{x}) = y v_0 / \sigma \exp[-(x^2 + y^2 + z^2)/\sigma^2],$$

$$v_y^0(\mathbf{x}) = -x v_0 / \sigma \exp[-(x^2 + y^2 + z^2)/\sigma^2].$$

Our simulations start with $\sigma = 0.07$ and $v_0 = 0.03$ in order to get results close to Marcus et al. (2013). This perturbation corresponds to a stratified anticyclonic vortex with a vertical vorticity $\omega_z = \partial_x v_y - \partial_y v_x \simeq -0.8$.

When using Kolmogorov-like noise, we randomly excite each velocity wavenumber isotropically in phase and amplitude and set the energy spectrum to $E(k) \propto k^{-5/3}$. We normalize our initial conditions so that $\sqrt{\langle v^2 \rangle} = 4 \times 10^{-2}$ at $t = 0$.

3 RESULTS

3.1 Fiducial case and hyperdiffusion

We first introduce our fiducial model h-256 (see Table 1) which essentially reproduces the results of Marcus et al. (2013). We choose a resolution of 256^3 Fourier modes in a cubic box representing a Keplerian disc with $q = 3/2$ and $\text{Fr} = 2$. Neither viscosity nor diffusion is imposed, $\nu = \chi = 0$. We instead use sixth-order hyperdiffusion to dissipate energy at small scales that would otherwise accumulate, spectral codes being inherently energy conserving schemes. We set

Table 1. List of simulations discussed in this Letter.

Run	Re	Pe	Re ₆	Pe ₆	τ	Resolution	ZVI
h-256-v	∞	∞	5×10^5	5×10^5	∞	256^3	Yes
h-1024-v	∞	∞	5×10^5	5×10^5	∞	1024^3	Yes
v6-1024-v	10^6	10^6	∞	∞	∞	1024^3	No
v7-1024-v	10^7	10^7	∞	∞	∞	1024^3	No
d5-256-v	∞	6.4×10^5	5×10^5	∞	∞	256^3	Yes
d4-256-v	∞	1.0×10^5	5×10^5	∞	∞	256^3	Yes
d4-256-k	∞	8.0×10^4	5×10^5	∞	∞	256^3	Yes
d3-256-v	∞	5.0×10^4	5×10^5	∞	∞	256^3	Yes
d3-256-k	∞	4.0×10^4	5×10^5	∞	∞	256^3	Yes
d2-256-v	∞	2.0×10^4	5×10^5	∞	∞	256^3	No
d2-256-k	∞	2.0×10^4	5×10^5	∞	∞	256^3	No
d1-256-v	∞	1.0×10^4	5×10^5	∞	∞	256^3	No
d1-256-k	∞	1.0×10^4	5×10^5	∞	∞	256^3	No
t5-256-v	∞	∞	5×10^5	∞	128	256^3	Yes
t4-256-v	∞	∞	5×10^5	∞	64	256^3	Yes
t4-256-k	∞	∞	5×10^5	∞	64	256^3	Yes
t3-256-v	∞	∞	5×10^5	∞	32	256^3	Yes
t3-256-k	∞	∞	5×10^5	∞	32	256^3	Yes
t2-256-v	∞	∞	5×10^5	∞	16	256^3	No
t2-256-k	∞	∞	5×10^5	∞	16	256^3	No

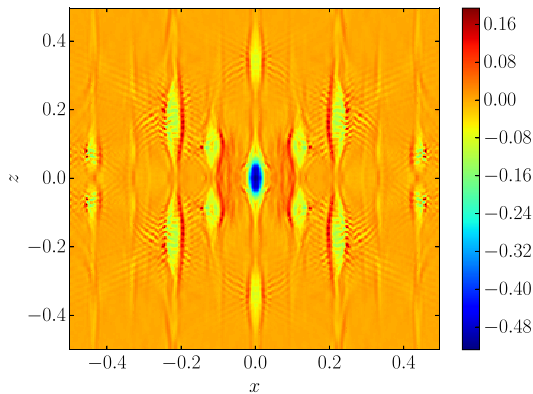


Figure 1. Vertical vorticity ω_z in a x - z cut of our fiducial simulation with $\text{Re}_6 = \text{Pe}_6 = 5 \times 10^5$ at $t = 500$. Similarly to Marcus et al. (2013), we observe the formation and replication of anticyclonic vortices on a fixed lattice.

$\text{Re}_6 = \text{Pe}_6 = 5 \times 10^5$. This simulation allows us to reproduce the main results of Marcus et al. (2013): self-replicating vortices on a fixed lattice (Fig. 1), and a growth in kinetic energy $E_K \equiv \langle v^2 \rangle / 2$ associated with these vortices (Fig. 2, blue line). As expected, new vortices appear at critical layers defined, from the initial vortex, by $x_c = \pm \text{Fr}L / (2\pi m q) \simeq \pm 0.21/m$, where m is the azimuthal mode number.

More interesting is the behaviour of these simulations when resolution and dissipation processes are modified. To illustrate this, let us consider higher resolution simulations with 1024^3 Fourier modes. We first perform a resolution test (h-1024) to reproduce our fiducial run *with hyperdiffusion* which confirms that our 256^3 run is numerically converged, at least with respect to E_K (Fig. 2, green line). We then restart this high-resolution simulation at $t = 400$ but revert to classical dissipation coefficients. We consider two cases: $\text{Re} = \text{Pe} = 10^6$ (v6-1024) and $\text{Re} = \text{Pe} = 10^7$ (v7-1024). The $\text{Re} = 10^6$ shows a clear and steep decay indicating that the ZVI disappears for this Reynolds number. If we move up to $\text{Re} = 10^7$, a decline is still seen, but we cannot say for sure that the ZVI is deactivated. A

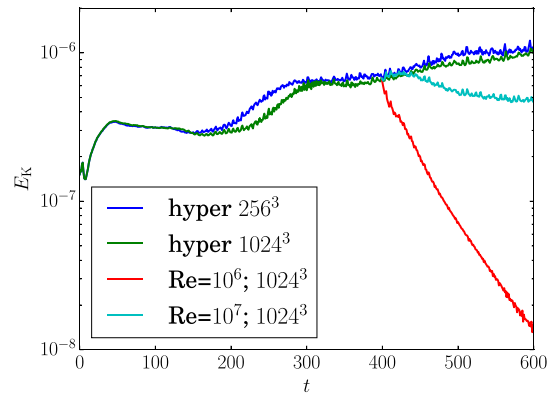


Figure 2. Volume averaged kinetic energy as a function of time for several simulations at $\text{Fr} = 2$ and $q = 3/2$. The blue curve corresponds to our fiducial case. High-resolution runs including diffusion are restarted from the hyperdiffusion run at $t = 400$.

careful examination of the critical layers at $t = 600$ in the $\text{Re} = 10^7$ case shows that they are resolved by only four to five collocation points (Fig. 3). We therefore conclude that the critical Reynolds number Re_c for the ZVI (if it exists) is certainly larger than 10^6 , and possibly larger than 10^7 . Simulations with at least 2048^3 (or even 4096^3) points will be required to confirm the existence of the ZVI with second-order dissipation operators.

3.2 Cooling and heating processes

The sensitivity to the Reynolds number indicates that the ZVI mechanism is highly dependent on dissipation and diffusion. In protoplanetary discs, Reynolds numbers are huge, so a high Re_c is not physically a problem (although it is definitely a problem for numerical simulations). Cooling in these discs, on the other hand, is far from negligible. It is therefore desirable to test the existence of the ZVI in the presence of cooling and heating.

In protoplanetary discs, cooling and heating are dominated by radiative transfer, thermal conductivity being unimportant.

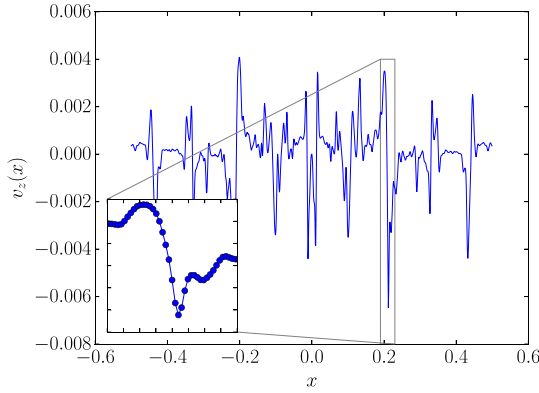


Figure 3. Vertical velocity as a function of x measured at $z = 0.1$ in run v7-1024-v at $t = 600$. The inset zooms on the critical layer at $x \simeq 0.21$ with dots representing the spectral collocation points. Note the sharpness of the critical layers despite the large resolution.

In optically thick regions, if the length-scales λ under consideration are larger than the photon mean free path $\ell_{\text{ph}} = 1/\kappa\rho$, where κ is the opacity and ρ is the gas density (i.e. the disc is optically thick on scale λ), cooling and heating can be approximated by thermal diffusion with a diffusion coefficient

$$\chi = \frac{16\sigma T^3}{3\kappa\rho^2 c_v}, \quad (4)$$

where σ is the Stefan–Boltzmann constant and c_v is the heat capacity of the gas, which we will assume to be diatomic. In the opposite limit $\lambda < \ell_{\text{ph}}$, radiative cooling acts like a scale-free Newtonian cooling with a characteristic time-scale t_c ,

$$t_c = \frac{\ell_{\text{ph}}^2}{3\chi}. \quad (5)$$

Note that *this cooling time-scale is not the same as the global cooling time-scale* of a vertically integrated disc (subject to external heating and radiative cooling), since here we look at *small-scale thermal perturbations* embedded in an optically thick medium. Similar estimates for the cooling function were obtained by Lin & Youdin (2015) for the VSI.

To illustrate the typical Peclet number and cooling times in protoplanetary discs, we have considered a typical T Tauri disc model $\Sigma = 140 R_{\text{au}}^{-1} \text{ g cm}^{-2}$ and $T = 280 R_{\text{au}}^{-1/2} \text{ K}$ which corresponds to a $0.01 M_{\odot}$ mass disc extending to 100 au. We assume the disc to be vertically isothermal as we do not solve the full radiative transfer equations. Rosseland opacities including gas and dust contributions are obtained from Semenov et al. (2003) assuming spherical homogeneous dust grains of solar composition. To compute the resulting Peclet number, we have identified the box scale L to the disc pressure scale height¹ $H \equiv c_s/\Omega$, where c_s is the local sound speed and Ω the local Keplerian frequency. The resulting map for thermal diffusion (Peclet number) is shown in Fig. 4. As mentioned above, the thermal diffusion approximation is valid only for scales $\lambda > \ell_{\text{ph}}$. The typical photon mean free path ℓ_{ph} is shown in Fig. 5. The smallest ℓ_{ph}/H is found close to the midplane in the inner parts of the disc. These are the regions expected to be well described by the

¹ In principle L can be arbitrarily smaller than H since we work in the incompressible limit. We have not considered this case since it leads to critical disc Pe even larger than the one discussed here, leading to a smaller domain of existence for the ZVI.

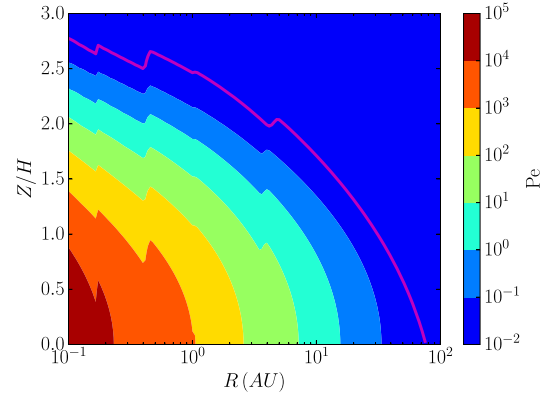


Figure 4. Peclet number as a function of position in a $0.01 M_{\odot}$ disc model. The magenta contour defines the $\tau = 1$ surface below which the disc is optically thick: $\ell_{\text{ph}} < H$.

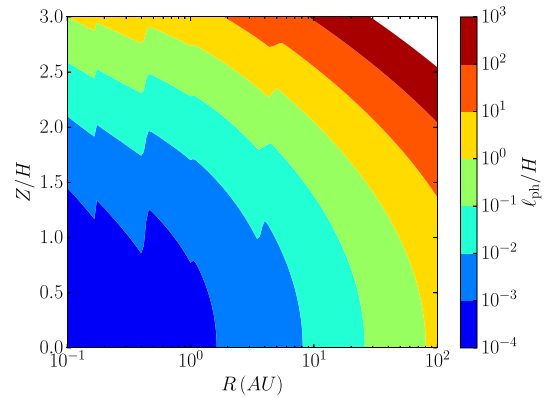


Figure 5. Photon mean free path ℓ_{ph} compared to the disc scale height H in a $0.01 M_{\odot}$ disc model. Shortest mean free paths are found close to the midplane in the innermost parts of the disc.

thermal diffusion approximation on most relevant scales.² On the contrary, the outer regions $R > 10 \text{ au}$ have $\ell_{\text{ph}} \lesssim H$. In these regions, cooling is best described by a constant cooling time characterized by the dimensionless parameter $\tau \equiv t_c \Omega$. Since the cooling time (equation 5) does not depend on density, τ is only a function of radius, shown in Fig. 6. From these three figures, we deduce that for $R \gtrsim 1 \text{ au}$, $\text{Pe} < 10^3$, and $\tau < 10^{-2}$. Note that in this discussion, we have only considered optically thick regions of the disc. Optically thin regions will likely have longer cooling time. However, they will also be affected by ionizing radiation which will allow MHD processes such as the MRI or winds to occur, making the ZVI irrelevant in these regions.

Our last task is to test in which parameter regime the ZVI lives. To this end, we have performed a set of simulations identical to our fiducial simulation, except that thermal hyperdiffusion is now replaced by a classical thermal diffusion operator with $\text{Pe} \in [10^4, 10^6]$ (runs dxxxx) or by a fixed cooling parameter $\tau \in [10, 200]$ (runs txxxx). We have used either the Gaussian vortex initial conditions (runs ending with ‘v’) or Kolmogorov noise initial conditions (runs ending with ‘k’). The energy evolution of the simulations starting

² Note however that the thickness of the critical layers involved in the ZVI can be several orders of magnitude smaller than the disc scale as it is set by gas molecular viscosity. It is therefore possible that critical layers are always in the optically thin regime for realistic Reynolds numbers.

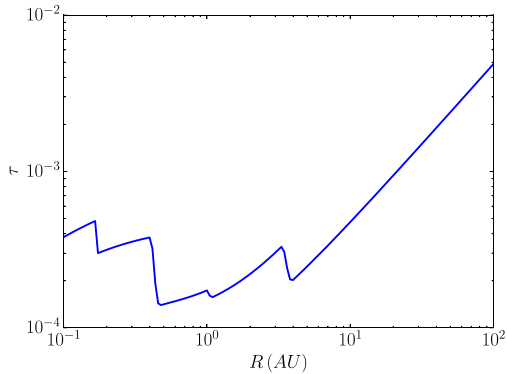


Figure 6. Dimensionless cooling time as a function of radius in a $0.01 M_{\odot}$ disc model. Jumps are due to the condensation of molecules on to dust grains which abruptly change opacities (Semenov et al. 2003).

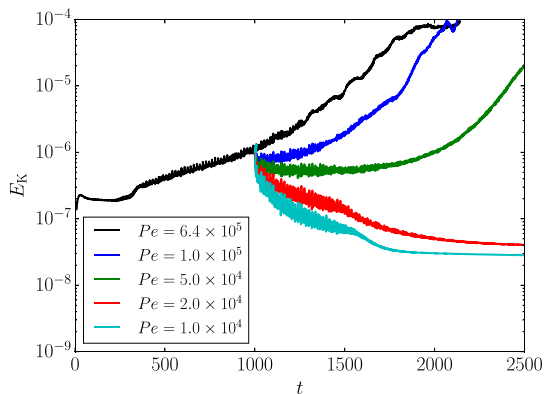


Figure 7. Volume averaged kinetic energy for runs dx-256-v varying thermal diffusivities. $Pe > 2 \times 10^4$ is needed to sustain the ZVI.

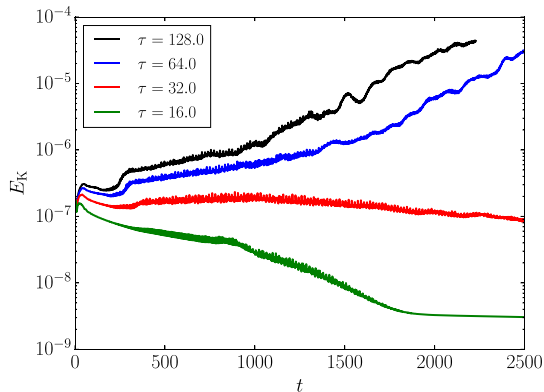


Figure 8. Volume averaged kinetic energy for runs tx-256-v varying thermal relaxation time-scales. $\tau > 16$ is needed to sustain the ZVI.

with a Gaussian vortex (Figs 7 and 8) clearly indicates that the ZVI requires $Pe > 2 \times 10^4$ and $\tau > 16$. Runs with $\tau \leq 16$ or $Pe \leq 10^4$ becomes axisymmetric at $t \sim 2000$ which ensure that the ZVI is definitely switched off for this range of parameters. Very similar limits are obtained when using Kolmogorov noise as an initial condition (Table 1). Our limits of existence for the ZVI therefore do not depend strongly on the chosen initial condition.

These dimensionless numbers are clearly excluded in our typical disc model presented above, except maybe in the diffusive regime in the innermost regions ($R \simeq 0.1$ au) which are also likely to be

unstable to the MRI due to their proximity to the central star (Latter & Balbus 2012).

4 CONCLUSIONS

In this Letter, we have explored the sensitivity of the ZVI to diffusive and thermal processes. We find that one can easily produce this instability with hyperdiffusion operators, but not with classical viscous operators. We conjecture that a resolution of at least 2048^3 collocation spectral points and a Reynolds number higher than 10^7 are required to ascertain the presence of the ZVI with physical dissipation. This should not come as a surprise since the instability mechanism relies on the physics of buoyancy critical layers, which are themselves controlled by diffusion (the process that sets their characteristic length-scale). It is therefore essential to properly resolve these structures with realistic dissipation operators (i.e. neither hyperdiffusion nor numerical dissipation). Note that finding the ZVI with finite volume codes does not solve this issue since these codes are also strongly affected by numerical diffusion.

We have also explored the sensitivity of the ZVI to cooling. If radiative diffusion or Newtonian cooling is too efficient then the action of buoyancy is diminished, as expected, and the instability switches off. The critical Peclet number below which ZVI fails is $\sim 10^4$, while the critical cooling time is $\sim 10\Omega^{-1}$. This critical Pe have been obtained with a fixed hyperdiffusivity so that the viscous scale is always much smaller than the thermal diffusion scale, as in a real protoplanetary disc. However, the ZVI may also show a dependence on $Pr = \nu/\chi$ or other combinations of dimensionless parameters. These dependencies have not been explored in this work.

Using a typical T Tauri disc model of $0.01 M_{\odot}$ mass, we find that the ZVI may struggle to survive except in the densest and innermost regions of the disc ($R \sim 0.1$ au) which are in any case MRI unstable. This is true whether the characteristic length-scale of the ZVI falls in the diffusive or Newtonian cooling regimes. Taken on face value, these results cast doubt on the ZVI as a potential source of turbulent transport and vortices in late-type objects (class II). We note, however, that younger discs ($M \sim 0.1 M_{\odot}$) or discs with steeper density profiles such as the minimum mass solar nebula (Hayashi 1981) could reach $Pe \sim 10^5$ at $R \lesssim 1$ au thanks to the increase in gas density. More massive discs would be subject to gravitational instabilities in their outer part but could be ZVI unstable in their inner part. Nevertheless, these scenarios must be confirmed by (a) demonstrating the existence and convergence of the ZVI with explicit viscous dissipation and (b) including a proper radiative transfer modelling to compute cooling accurately.

Note finally that this work has been performed in a local approximation (constant stratification, incompressibility, constant cooling). The ZVI being a local instability (Marcus et al. 2013, 2015), it is well captured and described by this model. Our study does not exclude the possibility of a *global* instability which would be due to the vertical structure of the disc. However, such a hypothetical instability would be driven by a different physical mechanism than that of the ZVI. Note also that global simulations will inherit (and probably exacerbate) the ZVI's numerical convergence problem (cf. Section 3.1).

ACKNOWLEDGEMENTS

The computations presented here were performed using the Froggy platform of the CIMENT infrastructure (<https://ciment.ujf-grenoble.fr>). HL acknowledges funding from STFC grant

ST/L000636/1 and helpful advice from John Papaloizou, Michael McIntyre, and Steve Lubow.

REFERENCES

- Balbus S. A., Hawley J. F., 1991, *ApJ*, 376, 214
 Barranco J. A., Marcus P. S., 2005, *ApJ*, 623, 1157
 Drazin P. G., Reid W. H., 1981, NASA STI/Recon Technical Report A, 82
 Dubrulle B., Marié L., Normand C., Richard D., Hersant F., Zahn J.-P., 2005, *A&A*, 429, 1
 Edlund E. M., Ji H., 2014, *Phys. Rev. E*, 89, 021004
 Gammie C. F., 1996, *ApJ*, 457, 355
 Hawley J. F., Gammie C. F., Balbus S. A., 1995, *ApJ*, 440, 742
 Hayashi C., 1981, *Progress Theor. Phys. Suppl.*, 70, 35
 Klahr H., Hubbard A., 2014, *ApJ*, 788, 21
 Latter H. N., Balbus S., 2012, *MNRAS*, 424, 1977
 Lesur G., Longaretti P.-Y., 2005, *A&A*, 444, 25
 Lesur G., Papaloizou J. C. B., 2010, *A&A*, 513, A60
 Lin M.-K., Youdin A. N., 2015, *ApJ*, 811, 17
 Lovelace R. V. E., Li H., Colgate S. A., Nelson A. F., 1999, *ApJ*, 513, 805
 Marcus P. S., Pei S., Jiang C.-H., Hassanzadeh P., 2013, *Phys. Rev. Lett.*, 111, 084501
 Marcus P. S., Pei S., Jiang C.-H., Barranco J. A., Hassanzadeh P., Lecoanet D., 2015, *ApJ*, 808, 87
 Nelson R. P., Gressel O., Umurhan O. M., 2013, *MNRAS*, 435, 2610
 Petersen M. R., Julien K., Stewart G. R., 2007, *ApJ*, 658, 1236
 Semenov D., Henning T., Helling C., Ilgner M., Sedlmayr E., 2003, *A&A*, 410, 611
 Turner N. J., Fromang S., Gammie C., Klahr H., Lesur G., Wardle M., Bai X.-N., 2014, in Beuther H., Klessen R. S., Dullemond C. P., Henning T., eds, *Protostars and Planets VI*. Univ. Arizona Press, Tuscan, AZ, p. 411
 Umurhan O. M., Shariff K., Cuzzi J. N., 2016, *ApJ*, in press, preprint ([arXiv:1601.00382](https://arxiv.org/abs/1601.00382))

This paper has been typeset from a \TeX/L\AA\TeX file prepared by the author.